ACS APPLIED MATERIALS & INTERFACES

Research Article

www.acsami.org

Low-Temperature Wet Conformal Nickel Silicide Deposition for Transistor Technology through an Organometallic Approach

Tsung-Han Lin,[†] Tigran Margossian,[†] Michele De Marchi,[‡] Maxime Thammasack,[‡] Dmitry Zemlyanov,[§] Sudhir Kumar,[†] Jakub Jagielski,[†] Li-Qing Zheng,[†] Chih-Jen Shih,[†] Renato Zenobi,[†] Giovanni De Micheli,[‡] David Baudouin,[†] Pierre-Emmanuel Gaillardon,[*,∥] and Christophe Copéret[*,†]

[†]Department of Chemistry and Applied Biosciences, ETH Zürich, Vladimir-Prelog-Weg 1-5, CH-8093 Zürich, Switzerland

[‡]Department of Electrical Engineering, EPF Lausanne, CH-1015 Lausanne, Switzerland

[§]Brick Nanotechnology Center, Purdue University, West Lafayette, Indiana 47907-2057, United States

[∥]Department of Electrical and Computer Engineering, University of Utah, Salt Lake City, Utah, 84112, United States

Supporting Information

ABSTRACT: The race for performance of integrated circuits is nowadays facing a downscale limitation. To overpass this nanoscale limit, modern transistors with complex geometries have flourished, allowing higher performance and energy efficiency. Accompanying this breakthrough, challenges toward high-performance devices have emerged on each significant step, such as the inhomogeneous coverage issue and thermal-induced short circuit issue of metal silicide formation. In this respect, we developed a two-step organometallic approach for nickel silicide formation under near-ambient temperature. Transmission electron and atomic force microscopy show the formation of a homogeneous and conformal layer of $NiSi_x$ on pristine silicon surface. Post-treatment decreases the carbon content to a level similar to what is found for the original wafer (~6%). X-ray photoelectron spectroscopy also reveals an increasing ratio of Si content in the layer after annealing, which is shown to be $NiSi_2$ according to X-ray absorption spectroscopy investigation on a Si nanoparticle model. *I*−*V* characteristic fitting reveals that this $NiSi_2$ layer exhibits a competitive Schottky barrier height of 0.41 eV and series resistance of 8.5 Ω, thus opening an alternative low-temperature route for metal silicide formation on advanced devices.

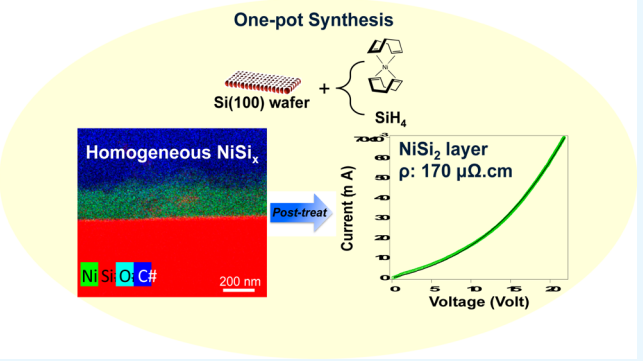

KEYWORDS: *nickel silicide, organometallic approach, one-pot synthesis, nanoparticle, surface investigation, semiconductor*

INTRODUCTION

For more than four decades, significant research efforts have been dedicated to the miniaturization of semiconductor devices in order to increase the amounts of transistors per cm^2 and enhance the performance of integrated circuits[1−5] with gate lengths of modern transistor technologies going down to 14 nm.[6−8] This evolution, namely the fastest in the history of modern industries, has also revealed that, in the near future, Moore's law[9] would be strongly challenged for the concern about processing and fabrication of the device with gate length below 14 nm. Recently, complex device structures with 3D geometries[2] have established themselves as the solution for the advanced generations of semiconductor devices.

Forming metal silicides, which are indispensable materials involved in the fabrication of all field-effect transistors,[10,11] has been identified as one of the major steps in modern process flows to reduce the contact resistance of the source and drain regions. Of metal silicides, nickel silicide ($NiSi_x$) is widely used by the industry because of its low resistivity, material compatibility, and good stability.[12−15] Several methods are employed to deposit nickel silicide thin films, which are generally formed using solid-state reactions of a metal species with silicon, such as physical vapor deposition (PVD),[13] chemical vapor deposition (CVD),[16,17] and atomic layer deposition (ALD).[18] However, with the shift to devices with even more complex 3D geometries,[19] conventional PVD method may no longer be the best choice for generating nickel silicide because of its lack of conformality, leading to the formation of inhomogeneous layers.[12] CVD and ALD are more promising candidates owing to the better aspect ratio attained compared with PVD method. Nevertheless, many challenges come from the thermal instability of nickel molecular precursors in gas-phase reaction, which limits the choices.[18,20]

Thus, forming homogeneous silicides in devices using complex 3D geometries is challenging by classical silicidation process. With this information in mind, we have investigated

Received: October 30, 2016
Accepted: January 12, 2017
Published: January 12, 2017

DOI: 10.1021/acsami.6b13852
ACS Appl. Mater. Interfaces 2017, 9, 4948−4955

Scheme 1. Schematic Representation of One-Pot Synthesis of $NiSi_x$ Layer on Si Substrate in This Work

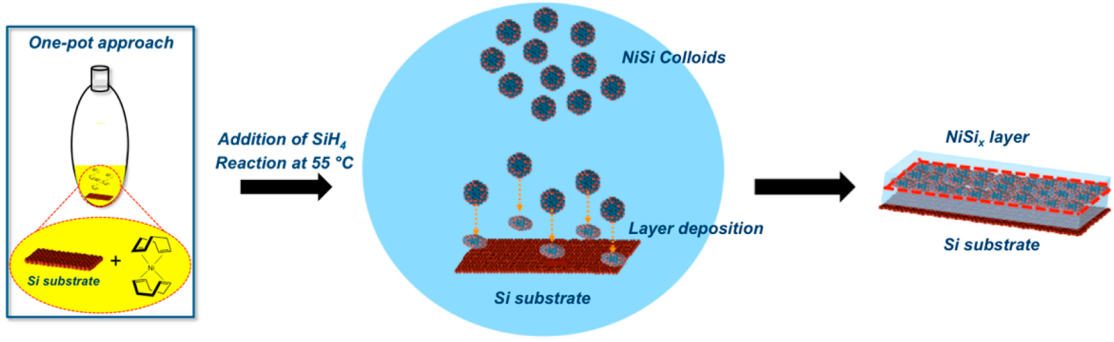

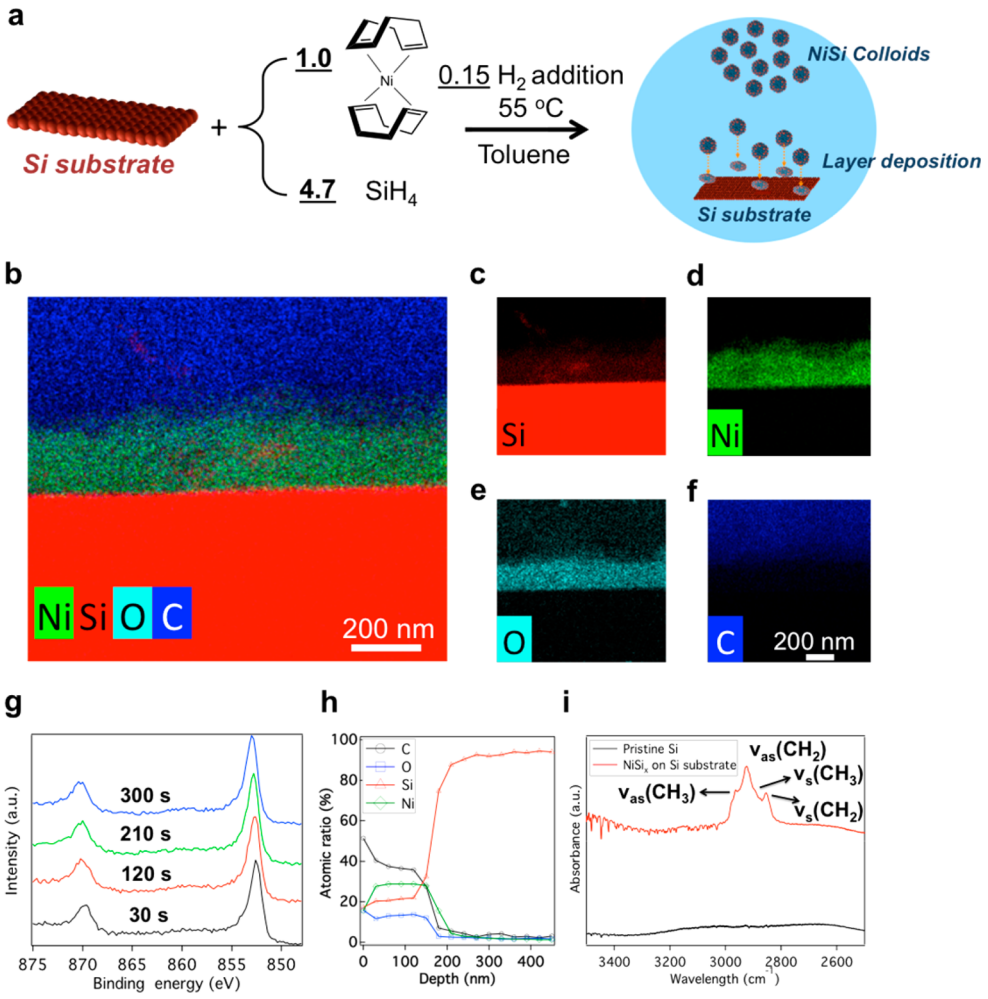

Figure 1. (a) Reaction scheme for one-pot synthesis, and the condition is as below: $Ni(COD)_2$/die, 110000 Ni·nm^{-2}, SiH_4/Ni = 4.7 with 0.01 mmol H_2, toluene, 55 °C for 16 h. (b) EDS mapping image of the Ni-rich layer on the Si substrate. (c–f) Si, Ni, O, and C EDS mapping images of the Ni-rich layer on the Si substrate, respectively. The wafer was exposed to air prior to EDS analysis. (g) X-ray photoelectron spectra of Ni 2p at different sputtering times, and (h) XPS depth profile quantization on the as-synthesized wafer. (i) Transmission FTIR spectra of the $NiSi_x$ layer on the as-synthesized wafer (red line), and the pristine Si wafer (black line).

the use of an alternative technique based on a wet chemical deposition method toward conformal and homogeneous deposition. This methodology takes advantage of recent developments in nickel-based colloidal nanoparticles production as catalysts for reforming applications,[21−23] where $NiSi_x$ colloids were obtained by reaction of bis(1,5-cyclooctadiene)-nickel(0) [$Ni(COD)_2$] and octylsilane at 55 °C.[24] Here, acutely aware of the application to microelectronic device fabrication, octylsilane was replaced by silane (SiH_4) in order to minimize the possible sources of organic contaminations in the layer. Based on this one-pot approach (Scheme 1), a homogeneous 200 nm Ni-rich layer was formed on the flat Si(100) substrate according to transmission electron microscopy (TEM) equipped with energy-dispersive spectroscopy (EDS). The layer was characterized by X-ray photoelectron spectroscopy (XPS) and atomic force microscopy (AFM), which showed the formation of a homogeneous Ni-rich film along with carbon deposit, that was mostly removed by annealing under H_2 flow

DOI: 10.1021/acsami.6b13852
ACS Appl. Mater. Interfaces 2017, 9, 4948−4955

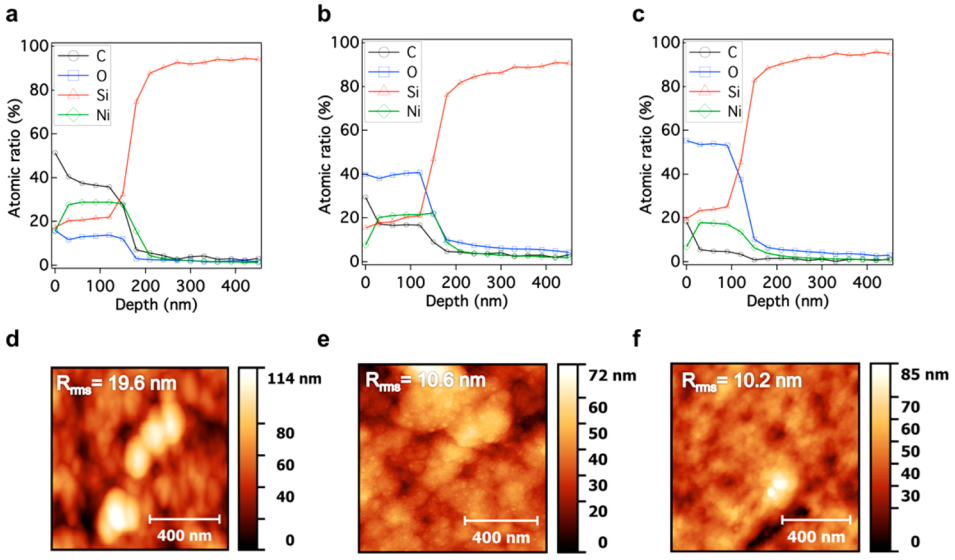

Figure 2. XPS depth profiles of Ni-rich layer on the Si substrate: (a) as-synthesized wafer; (b) wafer with post-treatment at 350 °C in H_2 flow; (c) wafer with post-treatment at 700 °C in H_2 flow. The atomic ratio was calculated in the first ∼120 nm. AFM images of Ni-rich layer on the Si substrate: (d) as-synthesized wafer in the scale of 1 μm^2, R_{rms} = 19.6 nm; (e) wafer with post-treatment at 350 °C in the scale of 1 μm^2, R_{rms} = 10.6 nm; (f) wafer with post-treatment at 700 °C in the scale of 1 μm^2, R_{rms} = 10.2 nm.

to a level similar to what is found for the pristine Si wafer (<9%). The annealing step generates $NiSi_2$ and an improvement of series resistance by 2 orders down to 8.5 Ω. According to these results and the isotropic nature of wet deposition, the disclosed processing approach may offer a solution for conformal nickel silicide formation on Si devices with complex 3D geometries, which is vital for modern semiconductor technologies.

RESULTS AND DISCUSSION

$NiSi_x$ Layer Deposited on Si Wafer by a Chemical Approach. A 40% HF treated (100) Si wafer (Figure 1a) was immersed in a dry and degassed solution of 0.07 mmol $Ni(COD)_2$ in toluene. The airtight container was then filled with 0.33 mmol SiH_4 and 0.01 mmol H_2 and let to react at 55 °C for 16 h under gentle stirring, yielding a homogeneous ca. 200 nm layer on top of the substrate along with a deep black solution (Figure 1b). The film was characterized by energy-dispersive X-ray spectroscopy (EDS) and XPS. Sample was exposed to air during transfers. EDS mapping shows that the layer contained Si (Figure 1c) and Ni (Figure 1d) along with oxygen (Figure 1e) and carbon (Figure 1f), vide infra for further discussions. The Ni core level was characterized by a binding energy around 853.2 eV, corresponding to the oxidized Ni (Ni^+ or Ni^{2+}) in the layer. In addition, the XPS depth profile (Figure 1h) shows the presence of carbon and oxygen (Si, Ni, C, and O atomic ratio average 23, 28, 36, and 13 at % in the first 150 nm) in the Ni-rich layer, which is consistent with the observation from EDS mapping (Figure 1b). However, the major peak for Si 2p at 103.2 eV (Figure S1) indicates that Si is partially oxidized in this layer, probably in the form of $NiSi_xO_y$ formed upon exposure to air during the ex situ transferring to the XPS chamber (see the Supporting Information). To understand the origin of contaminations, we conducted the XPS analysis of a pristine wafer to serve as a background reference (Figure S2). Its depth profile analysis shows that the average surface atomic ratio of oxygen is ∼5 at % (Table S1), which is consistent with the formation of surface oxide. However, the surface atomic ratio of carbon on the pristine wafer is ∼18 at %, which is much less than in the as-synthesized thin film. It can hence be concluded that the presence of oxygen mainly results from the exposure to air during the ex situ transferring to the XPS chamber, while carbon probably comes from the synthetic approach, as shown by transmission Fourier transform infrared spectroscopy (FTIR) carried out under inert conditions (Figure 1i). After the one-pot chemical reaction, signals of C−H bands were observed in the 2800−3000 cm^{-1} region in agreement that the carbon contamination observed in XPS (single C 1s peak at 284.8 eV) was mostly present as alkyl groups. It probably originates from the hydrosilylation reaction of SiH_4 and the olefinic group of the cyclooctadiene ligand of $Ni(COD)_2$, which forms Si−C bonds.[25]

Annealing under H_2. Because of the presence of residual alkyl groups, a post-treatment under H_2 flow at high temperature was performed. After post-treatment, XPS depth profiling (Figure 2b, c) reveals that the carbon amount decreased with increasing temperature of post-treatment; from 36 to 17 and 5 at % at 350 and 700 °C, respectively (Table 1). It is worth noting that, after post-treatment at 700 °C, the amounts of carbon dropped down to ∼5 at% which corresponds to the background level (Figure S2a). In parallel, this layer became thinner (Figure 2c) and the Si/Ni ratio was increased from 0.8 to 1.8, consistent with the formation of $NiSi_2$ (vide infra for characterization of the layer). This change

Table 1. Quantitative XPS Depth Profiles of Ni-Rich Layer on the Si Substrate

condition	nickel (at %)	silicon (at %)	carbon (at %)	oxygen (at %)
As-syn[a]	28	23	36	13
PO_350[b]	21	19	17	40
PO_700[c]	16	29	5	50

[a]As-synthesized sample. [b]Sample after post-treatment at 350 °C. [c]Sample after post-treatment at 700 °C. All atomic ratios were averaged in the first 120 nm.

DOI: 10.1021/acsami.6b13852
ACS Appl. Mater. Interfaces 2017, 9, 4948−4955

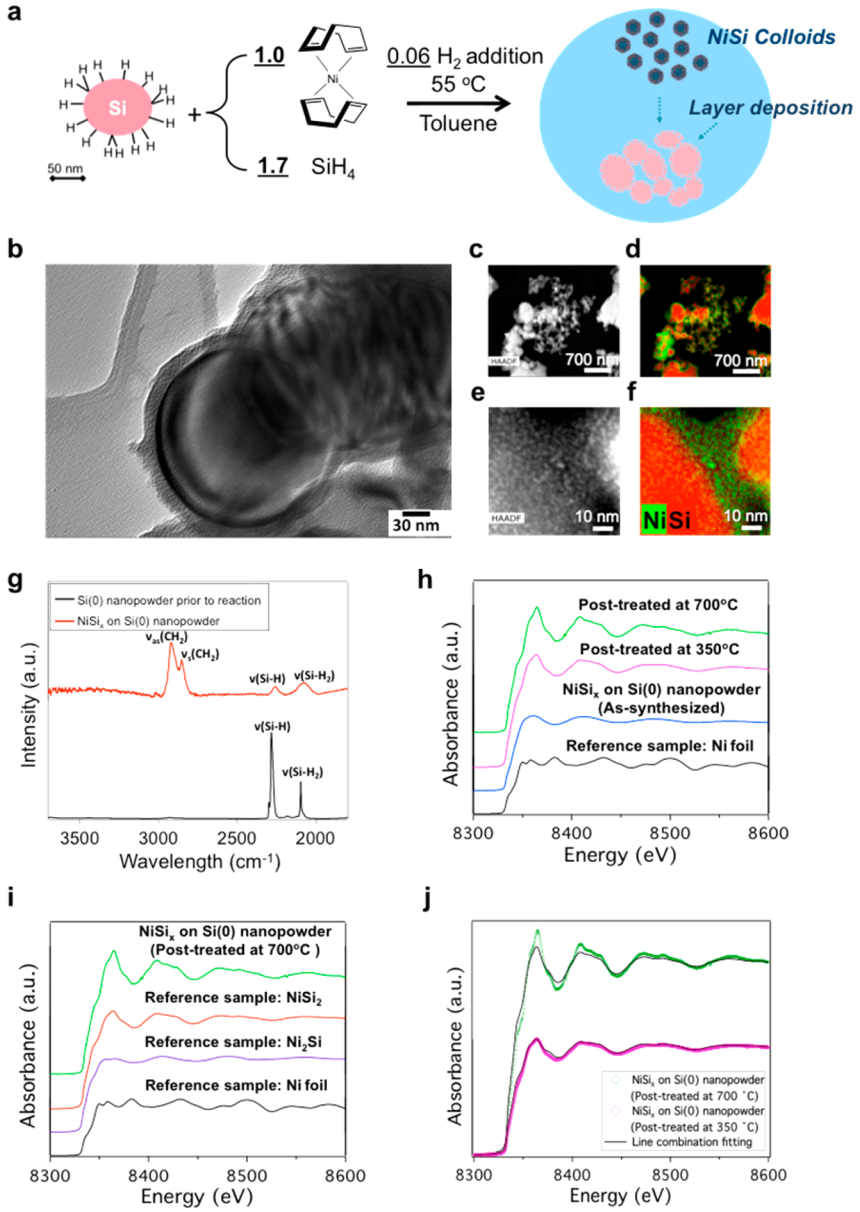

Figure 3. (a) Reaction scheme of the one-pot synthesis for Ni-rich layer on Si(0) nanopowder. (b) HRTEM analysis of $NiSi_x$ on the Si(0) nanopowder ($Ni(COD)_2$ 350 Ni/nm^2, SiH_4/Ni = 1.7, toluene, 55 °C, without post-treatment). (c) High-angle annular dark-field (HAADF) image of $NiSi_x$ on the Si(0) nanopowder with (d) Ni and Si maps. (e) Zoom-in HAADF image of $NiSi_x$ on the Si(0) nanopowder with (f) Ni and Si maps. (g) FTIR analysis of nanopowder: Black, Si(0) after H_2 regeneration; red, $NiSi_x$ on the surface after one-pot synthesis. (h) X-ray absorption spectra of samples of $NiSi_x$ on Si(0) nanopowder and Ni (0) foil as the reference (black line). (i) X-ray absorption spectra of Si(0) nanopowder after 700 °C post-treatment and references. (j) Linear combination fitting of $NiSi_x$ on Si(0) nanopowder after 350 °C (pink curve) and 700 °C (green curve) post-treatment with the reference of Ni(0), $NiSi_2$, and Ni_2Si.

results from the diffusion of Ni atoms into Si substrate along with Si atoms diffusing out at higher temperatures, thus inducing the phase transformation.[14] Note that there is a sharp increase in Si content with a decrease in Ni content in the interface (depth ~150 nm) for all samples, after which the values are associated with bulk Si substrate.

Concerning the presence of oxygen, it increases with increasing temperature of post-treatment and parallels the decrease amount of carbons. As discussed in the previous part, it is likely related to the oxidation of the layer upon transferring of the wafer to the XPS chamber.

To correlate this composition difference to surface morphology, we conducted AFM, which showed the value of root-mean-square roughness (R_{rms}) of as-synthesized wafer is 19.6 nm (Figure 2e). However, samples after post-treatment showed R_{rms} equaled to 10.6 nm (Figure 2e) and 10.2 nm (Figure 2f) at 350 and 700 °C, respectively. Combined with XPS results, post-treatment under H_2 flow at high temperature effectively decreased the carbon amount down to the level similar to pristine Si wafer and allowed for the formation of a homogeneous $NiSi_2$-like layer by the increasing Si/Ni ratio to 1.8 (Table 1), which will be further analyzed and proved by the X-ray absorption spectroscopy (XAS) on a model of Si(0) nanoparticles in the following part.

Characterization of $NiSi_x$ Layer Using Si Nanoparticles As a Model. To further clarify the nature of the layer on top of Si wafer, we used Si(0) nanoparticles as a model in order to broaden the surface characterization by FTIR[26] and XAS.

DOI: 10.1021/acsami.6b13852
ACS Appl. Mater. Interfaces 2017, 9, 4948−4955

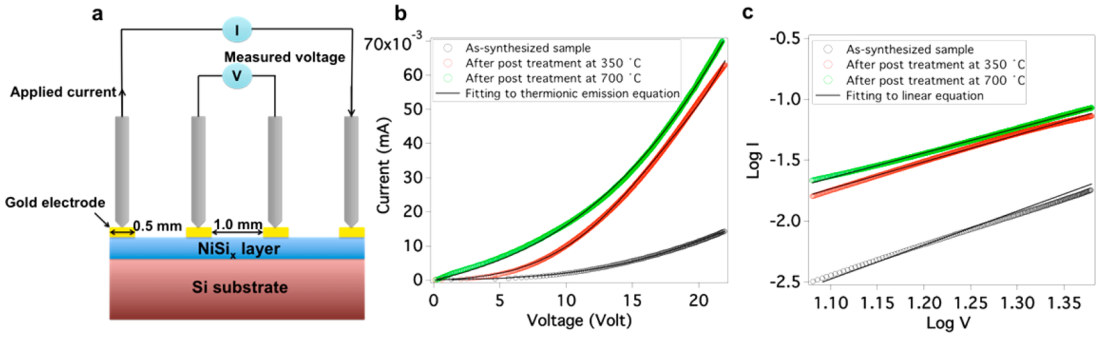

Figure 4. (a) Schematic device for the four-point probe measurement (b) $I-V$ characteristics of $NiSi_x$ layer on the Si(100) wafer fitting to thermionic emission equation. Black circles, as-synthesized wafer; red circles, sample after 350 °C post-treatment; green circles, sample after 700 °C post-treatment; black lines, thermionic emission equation fitting curves. (c) Logarithmic plots are acquired by the $I-V$ curve in b) and fitted to a linear equation.

The one-pot chemical approach described above was used on Si(0) nanoparticles, which were previously treated at 900 °C under H_2 to provide a surface solely terminated by Si−H as for wafers (Figure S3). The targeted surface Ni loading was lower than that for the wafer: 350 Ni·nm^{-2} instead of 110 000 Ni·nm^{-2}. The reaction of $Ni(COD)_2$ and SiH_4 with the addition of H_2 at 55 °C on the Si(0) nanoparticles (Figure 3a) also leads to the formation of a homogeneous layer throughout the surface of these spherical nanoparticles, whose thickness was ca. 15 nm according to high-resolution TEM (HRTEM) (Figure 3b). EDS mapping of high magnification (Figure 3f) showed this layer was composed of Ni and Si and covered on the entire surface of Si(0) nanoparticles, which was consistent with the layer formed on the Si wafer in the previous part. FTIR analysis was carried out on the as-synthesized sample after proper washing under inert condition and drying under high vacuum (~10^{-5} mbar). While, before reaction, there is an intense peak at 2280 and 2100 cm^{-1} associated with Si−H and Si−H_2 on top of the Si(0) nanoparticles (black line of Figure 3g), this band mostly disappears after the deposition of $NiSi_x$ (red line of Figure 3g), which is consistent with the consumption of the Si−H bonds. FTIR also showed that C−H signals appeared on the surface after reaction. These bands at 3000 cm^{-1} to 2800 cm^{-1} correspond to alkyl groups, which are presumably originated from the COD ligand of $Ni(COD)_2$ and possibly through the hydrosilylation of COD.[25] Combined with HRTEM and EDS mapping images (Figure 3b and 3f), these data indicate that a homogeneous Ni-rich layer was formed on the surface of Si(0) nanoparticles. All the data are consistent with what is observed on wafers.

To understand the nature of the $NiSi_x$ layer formed on the surface, we carried out Ni K-edge XAS under Ar, and the corresponding spectrum for as-synthesized Ni-rich layer on Si(0) nanopowder (blue curve, Figure 3h) presents significantly different constructive and destructive interferences compared with Ni(0) foil reference (black curve, Figure 3h). Combined with XPS results, the observed edge shift of 0.4 eV at the Ni K-edge with respect to Ni(0) foil indicates that this film is composed of $NiSi_x$ instead of Ni(0), and the energy shift is attributed to the charge redistribution for the $NiSi_x$ formation.[27] For the samples after post-treatment at 350 and 700 °C (Figure 3h), the observed edge shifts are 0.9 and 1.8 eV with respect to Ni(0) foil, which revealed that the Ni went through the phase transformation to higher oxidative state. Furthermore, linear combination fitting of XAS was conducted on $NiSi_x$ after 350 and 700 °C post-treatment and compared with the reference samples of $NiSi_2$, Ni_2Si, and Ni(0) foil (Figure 3i and 3j). It showed that for the sample post-treated at 350 °C, the fit is consistent with the presence of ca. 95% $NiSi_2$ and 5% Ni(0), whereas after post-treatment at 700 °C, the data perfectly fit to $NiSi_2$ reference sample. The fitting results confirm the observation from previous XPS results (Figure 2) that phase transformation occurred during post-treatment and that this Ni-rich layer was mainly composed of $NiSi_2$ after post-treatment at 700 °C.

***I−V* Characteristics of $NiSi_x$ on Si(100) Wafer.** In order to gain insight into the $NiSi_x$ layer, the current (I)−voltage (V) characteristics were measured by the four-point probe setup, as shown in Figure 4a and $I-V$ curve in Figure 4b. Rather than the Ohmic behavior, the $I-V$ curve is reminiscent of a nonideal diode, which suggests a Schottky barrier with the rectifying behavior in the layer, presumably resulting from the ensemble of junctions between the individual $NiSi_x$ nanoparticles (Figure S4). Accordingly, the thermionic emission model (1)[28,29] was adopted to fit the positive part of $I-V$ characteristics, given by

$$I_a = AA_0T^2e^{-\Phi_n/k_BT}[e^{-e_0(V-R_sI_a)/\eta k_BT} - 1] \quad (1)$$

where I_a is applied current (A), V is measured voltage (V), A is active area (7.8×10^{-7} m^2), A_0 is effective Richardson constant (1.20×10^6 A·m^{-2}·K^{-2}), T is temperature of the junction (298 K), k_B is the Boltzmann constant (8.62×10^5 eV/K), Φ_n is Schottky barrier height (eV), η is the ideality factor, and R_s is the series resistance (Ω) (see the Supporting Information for calculation method).

For the as-synthesized sample, the fitted Schottky barrier height and the series resistance are 0.51 eV and 371.8 Ω, respectively, with the ideality factor of 157 (Table 2). Following the same fitting procedure, Schottky barrier heights after post-treatment at 350 and 700 °C significantly decrease to 0.49 and 0.41 eV; similarly, the series resistances decrease to 130.9 and 8.5 Ω. The ideality factors, on the other hand, remain within the same order of magnitude (107 and 394), indicating a

Table 2. $I-V$ Characteristics of $NiSi_x$ on the Si(100) Wafer

condition	Φ_n (eV)	R_s (Ω)	η	Log I/Log V
As-syn[a]	0.51	371.8	156.7	2.8
PO_350[b]	0.49	130.9	106.7	2.2
PO_700[c]	0.41	8.5	393.8	2.1

[a]As-synthesized sample. [b]Sample after post-treatment at 350 °C. [c]Sample after post-treatment at 700 °C.

DOI: 10.1021/acsami.6b13852
ACS Appl. Mater. Interfaces 2017, 9, 4948−4955

nonideal $I-V$ behavior for $NiSi_2$ prepared by the chemical method. The higher barrier and series resistance of as-synthesized wafer are probably resulted from the presence of organic residues and the amorphous layer formed by the chemical method. The post-treatment at high temperature eliminates the organic residues, decreases the carbon content and improves surface roughness as shown by the XPS and AFM results (Figure 2), thus allowing a lower series resistance down to 8.5 Ω (170 μΩ.cm for resistivity). However, compared with the reported resistivity of $NiSi_2$ layer by CVD method (36 μΩ cm),[11] the higher resistivity and ideality factor suggest the presence of more resistive domains, possibly voids, between $NiSi_2$ nanoparticles, resulted from the removal of carbon contamination and the diffusion of Ni atoms by the post-treatment. This phenomenon can be also evidenced by the XPS depth profile (Figure 2a–c). After post-treatment at 350 and 700 °C, the oxygen ratio increases from 13% to 40% and 50%, respectively (Figure 2b, c). However, voids are formed upon removal of carbon contamination (carbon content decreases from 36 to 5 at %), allowing more oxygen to diffuse in this layer. In the same time, due to the diffusion of Ni atoms into the substrate (Ni content decrease from 28 to 16 at %), the layer becomes thinner with more voids, as shown by the TEM-EDS mapping image (Figure S5). Thus, the $NiSi_2$ layer is composed of the intercalation of nanoparticles as electron traps and resistive domains, in which the current conduction comes from charges jumping over barriers in between these nanoparticles. This is corroborated by the behavior of space charge limited current, proved by the ratio of Log I/Log V is close to 2 in Figure 4c,[30] which leads to an overall higher resistance and ideality factor of the $NiSi_2$ material prepared by the chemical method.

CONCLUSIONS

In this study, a one-pot chemical approach was developed to deposit $NiSi_2$ layer on Si wafer with competitive Schottky barrier and resistivity. This $NiSi_2$ layer was formed in two steps through (1) the formation of a homogeneous nickel silicide layer upon reaction of $Ni(COD)_2$ and SiH_4 with the wafer surface at low temperature, here 55 °C, followed by (2) a post-treatment under H_2 at 700 °C, yielding a $NiSi_2$ layer according to XPS and XAS analysis. This post-treatment removes organic residues and allows a lower Schottky barrier of 0.41 eV and resistivity of 170 μΩ·cm. Furthermore, using trenched Si wafer and the same one-pot synthetic approach (Figure S6), TEM-EDS mapping of the as-synthesized sample shows the deposition of an homogeneous layer on top of the trenched structure with the step coverage of 0.74, which is comparable to what is obtain by CVD method, thus showing that this method can be applied to more complex structures. In summary, this method provides another route for the deposition of metal silicide at low temperature, and it has the advantage to be easily applied to 3D structures by conformal deposition on state-of-the-art semiconductor devices.

METHODS

General Information. The experiments were carried out by Schlenk techniques and in a mBraun LABstar glovebox under an argon atmosphere. Toluene was dried and collected using a mBraun SBS-800 purification system and degassed by Schlenk techniques (vacuum to 10^{-1} mbar and sparge with dry Ar for 10 times). 40% HF solution was purchased from VWR. Si(0) nanopowder was purchased from US-nano with the size between 20 and 30 nm and with 98% purity. $Ni(COD)_2$ were purchased from Strem and used as received. 1% SiH_4 (N5.0) in helium was purchased from PanGas. Pure H_2 (N5.0) gas was also purchased from PanGas. Every glassware was oven-dried for at least 4 h prior to use at temperatures greater than 150 °C.

Nickel Silicide Colloidal Nanoparticle Synthesis on Si Wafer (One-Pot Synthesis). First, p-type double-polished 4 in. Si wafers with (100) orientations were diced into 2 cm × 1 cm dies and cleaned by 40% HF solution for 60 s. The diced wafers were then dried in a high vacuum (~1×10^{-5} mbar) Schlenk line for 12 h.

Second, one diced Si wafer and 20 mg of $Ni(COD)_2$ (0.07 mmol) were placed in a 325 mL reactor in the glovebox. Then, the reactor was connected to Schlenk line and 10 mL toluene was injected into the reactor at room temperature until all $Ni(COD)_2$ were dissolved under gentle stirring. Then, 2.7 bar of 1% SiH_4 (0.33 mmol) was put into the reactor at room temperature and 0.01 mmol of H_2 was put in the reactor. After that, the temperature was raised to 55 °C. After 16 h, there was a layer on top of the substrate and the formation of colloidal solution (dark solution formed). The colloidal solution was transferred out of the reactor and the as-synthesized wafer was washed for 2 times in the reactor with 10 mL dry toluene. Finally, the wafer was dried in vacuum (~1×10^{-2} mbar) for 3 h, and the reactor was transferred into the glovebox so that the as-synthesized wafers could be stored and analyzed in the inert condition.

Nickel Silicide Colloidal Nanoparticle Synthesis on Si(0) Nanopowder (One-Pot Synthesis). First, Si(0) nanopowders were treated with 900 °C in H_2 flow for 12 h to remove the surface silica and regenerate Si–H bond on it (Figure S3).

Second, 50 mg of Si(0) nanopowders and 73 mg of $Ni(COD)_2$ (0.27 mmol) were put in the 325 mL reactor in the glovebox. Then, the reactor was connected with Schlenk line and 10 mL of toluene was injected into the reactor at room temperature until all $Ni(COD)_2$ were dissolved under stirring. Then, 3.5 bar of 1% SiH_4 (0.45 mmol) was put into the reactor under room temperature and 0.01 mmol H_2 were put in the reactor. After that, the temperature was raised to 55 °C. After 16 h, the solution was composed of dispersed silicon nanopowders and black colloidal solution (sub-10 nm nanoparticles). The reactor was transferred into the glovebox and the silicon nanopowders were washed with 10 mL of dry toluene and filtered 3 times. Then, the as-synthesized nanopowders were dried in high vacuum (~1×10^{-5} mbar) for 3 h.

Post-Treatment Condition. As-synthesized wafer/nanopowders was treated at high temperature (350 or 700 °C) under a pure H_2 flow at 950 mbar for 12 h.

Characterization Techniques. TEM and EDS images were taken with a FEI Tecnai Orisis ultrahigh vacuum transmission electron microscope. The AFM measurements were conducted on a commercial AFM system (BioScope Catalyst, Bruker Nano, Santa Barbara, California) that is mounted onto an inverted confocal laser-scanning microscope (FluoView FV500, Olympus, Center Valley, Pennsylvania). The images shown in this study were obtained using tapping mode AFM with CT300R-25 cantilever probes (Nanoscience, USA). The AFM images are 1 μm in size, with a resolution of 256 × 256 pixels, and a scan rate of 0.2 Hz. FTIR spectra of wafers were recorded in transmission mode on Thermo Scientific, Nicolet 6700, in which the measurements were performed under inert condition with a deuterated triglycine sulfate (DTGS) detector with 1000 averaged scans to achieve an optimal signal-to-noise ratio. FTIR spectra of nanopowders were recorded in transmission mode on a Bruker ALPHA-T FTIR spectrophotometer under inert condition.

XPS depth profiles were obtained using a Kratos Axis Ultra DLD spectrometer with monochromic Al Kα radiation (1486.6 eV). A commercial Kratos charge neutralizer was used to avoid non-homogeneous electric charge and to achieve better resolution. The resolution measured as full width at half-maximum of the curve fitted photoemission peaks was approximately 1 eV. Binding energy (BE) values refer to the Fermi edge and the energy scale was calibrated using Au $4f_{7/2}$ at 84.0 eV and Cu $2p_{3/2}$ at 932.67 eV. Samples were attached to a stainless steel sample holder bar using a double-sided sticking Cu tape. XPS data were analyzed with CasaXPS software version 2313 Dev64 (www.casaxps.com). The C–C component of the

DOI: 10.1021/acsami.6b13852
ACS Appl. Mater. Interfaces 2017, 9, 4948–4955

C 1s peak was set to a binding energy of 284.8 eV to correct for charge on each sample. Curve-fitting was performed following a linear or Shirley background subtraction using Gaussian/Lorentzian peak shapes. The atomic concentrations of the elements in the near-surface region were estimated taking into account the corresponding Scofield atomic sensitivity factors and inelastic mean free path (IMFP) of photoelectrons using standard procedures in the CasaXPS software. Depth profiling was conducted by step by step sputtering of a sample with a Kratos polyatomic sputtering gun operating in Ar mode at 5 keV, $I_{ion} \approx 1$ μA. Thickness of the layers was calibrated using the TEM measured thickness.

Ni 2p and Si 2p XPS spectra were acquired by an ESCA KRATOS AXIS ULTRA, which were performed using a monochromatic Al K_α (1486.6 eV) X-ray source (chamber under high vacuum). XPS spectra were fitted by the Gaussian−Lorentzian function after subtraction of baseline (Shirley baseline).

XAS data were carried out at the X10DA (Super XAS) beamline at the Swiss Light Source, Villigen, Switzerland. Spectra were collected on pressed pellets optimized to 1 absorption length at the Ni K-edge in transmission mode. The beamline energy axis was calibrated with a Ni reference foil, in which energies are measured at the inflection point(s) of the absorption signal, and the precision on the energy of the edge is ±0.5 eV in the (8303−8373 eV) area. The spectra were background-corrected using the Athena software package. Linear combination fits were performed by the routine of Athena software[31] over the range of 8300 to 8600 eV using reference spectra of Ni(0) foil, Ni_2Si, and $NiSi_2$.

For four-point probe measurement, four 100 nm gold (Au) electrodes were evaporated to a circle-shape layer (0.25 mm in radius; separate with each one by 1 mm) with a deposition rate of 5 ± 2 Å. s^{-1} by thermal evaporation of Au ingots under high vacuum (~1 × 10^{-5} mbar). The Au ingots (99.999%) were supplied by Kurt J. Lesker. A MBraun glovebox integrated MBraun vacuum thermal evaporator was used for the Au evaporation. The probe station used for I−V characteristic measurement is a Signatone S1160, and the *I*−*V* data were acquired by a Keysight B1500 with B1510A High Power source/monitor unit (HPSMU).

TEM Sample Preparation by Tripod Method. The as-synthesized wafer was cleaved into two pieces of 2.5 × 1.8 mm. These two pieces were then glued face-to-face with a Gatan G2 epoxy glue, in which the face to be observed was in the middle.

The procedure to complete polishing had two steps. First, the specimen was mounted on the side of a tripod polisher using Quickstick at 100 °C. A polishing of one side to remove most of the bulk materials was processed by a series of plastic diamond lapping films, with grains of decreasing sizes (30, 15, 6, 1, 0.5, and 0.1 μm) and a final step was done on a soft felt covered disc impregnated with silica of 25 nm grain size.

Second, the specimen was mounted on the bottom of a tripod polisher using Quickstick at 100 °C. In this step, the glass support has to be perfectly flat polished to ensure a correct 0.6° angle of the wedge shape of the specimen. The flat polishing of the glass also prevented from bubble formation in the Quickstick that would break the specimen when the thickness is down to 100 nm. Also, this step was processed by a series of plastic diamond lapping films, with grains of decreasing sizes (30, 15, 6, 1, 0.5, and 0.1 μm) and a final step was done on a soft felt covered disc impregnated with silica of 25 nm grain size. The specimen is ready when interference fringes can be observed on it, proving its electron transparency.

Finally, the specimen was glued on a Mo grid with a diameter adapted to the holder of the microscope. After one night of drying, the grid was detached from the tripod using acetone to dissolve the Quickstick, and the specimen was cleaned.

■ ASSOCIATED CONTENT

Supporting Information

The Supporting Information is available free of charge on the ACS Publications website at DOI: 10.1021/acsami.6b13852.

Supporting experimental data, FTIR, XPS, XAS (PDF)

■ AUTHOR INFORMATION

Corresponding Authors

*E-mail: pierre-emmanuel.gaillardon@utah.edu.

*E-mail: ccoperet@inorg.chem.ethz.ch.

ORCID

Chih-Jen Shih: 0000-0002-5258-3485

Christophe Copéret: 0000-0001-9660-3890

Author Contributions

P.-E.G, D.B., C.C., and G.D.M. conceived the project. T.L., T.M., D.B, P.-E.G., and C.C. designed all experiments. T.L. wrote the manuscript, prepared figures, performed *I*−*V* characteristics measurements and data fitting. T.L., T.M., and D.B. did chemical reactions and treatments, surface analysis. M.D.M. and M.T. prepared samples and conducted TEM-EDS/XPS analysis. D.Z. performed XPS analysis. S.K. conducted the electrode evaporation for four-point measurement. J.J. helped write code for matlab fitting. L.Z. carried out AFM analysis with the supervision of R.Z. P-E.G. and C.S. gave suggestions on I−V characteristics explanation. C.C., P.-E.G., D.B., and G.D.M. revised the manuscript. All authors reviewed the manuscript.

Notes

The authors declare no competing financial interest.

■ ACKNOWLEDGMENTS

The authors thank the financial support by ChemNiSi project of Swiss National Science Foundation grant CR22I2_152955 and by grant 1644592 of the US National Science Foundation. ETH Zürich, EPF Lausanne, and The University of Utah are also acknowledged for funding, scientific support, and the access to the process and characterization facilities. We also thank Frank Krumeich (ETHZ) for his precious help with HRTEM, Ribeiro Fabio (Purdue Catalysis Center, Purdue University) for his help with XPS, and Christoph Müller (ETHZ) and Wouter VanBeek (ESRF) for their support for XAS measurement.

■ REFERENCES

(1) Hisamoto, D.; Lee, W.-C.; Kedzierski, J.; Takeuchi, H.; Asano, K.; Kuo, C.; Anderson, E.; King, T.-J.; Bokor, J.; Chenming, H. FinFET-A Self-Aligned Double-Gate MOSFET Scalable to 20 nm. *IEEE Trans. Electron Devices* **2000**, *47* (12), 2320−2325.

(2) Guo, J.S.; Xiang, Q.; Takamura, Y.; Wang, H.; Pan, J.; Arasnia, F.; Paton, E. N.; Besser, P.; Sidorov, M. V.; Adem, E.; Lochtefeld, A.; Braithwaite, G.; Currie, M. T.; Hammond, R.; Bulsara, M. T.; Lin, M.-R. Scalability of Strained-Si nMOSFETs Down to 25 nm Gate Length. *IEEE Electron Device Lett.* **2003**, *24* (5), 351−353.

(3) Iwai, H. Roadmap for 22 nm and Beyond. *Microelectron. Eng.* **2009**, *86* (7−9), 1520−1528.

(4) Ng, H. T.; Han, J.; Yamada, T.; Nguyen, P.; Chen, Y. P.; Meyyappan, M. Single Crystal Nanowire Vertical Surround-Gate Field-Effect Transistor. *Nano Lett.* **2004**, *4* (7), 1247−1252.

(5) Xiang, J.; Lu, W.; Hu, Y.; Wu, Y.; Yan, H.; Lieber, C. M. Ge/Si Nanowire Heterostructures as High-Performance Field-Effect Transistors. *Nature* **2006**, *441* (7092), 489−493.

(6) Lin, C. H.; Greene, B.; Narasimha, S.; Cai, J.; Bryant, A.; Radens, C.; Narayanan, V.; Linder, B.; Ho, H.; Aiyar, A.; Alptekin, E.; An, J. J.; Aquilino, M.; Bao, R.; Basker, V.; Breil, N.; Brodsky, M.; Chang, W.; Clevenger, L.; Chidambarrao, D.; Christiansen, C.; Conklin, D.; DeWan, C.; Dong, H.; Economikos, L.; Engel, B.; Fang, S.; Ferrer, D.; Friedman, A.; Gabor, A.; Guarin, F.; Guan, X.; Hasanuzzaman, M.; Hong, J.; Hoyos, D.; Jagannathan, B.; Jain, S.; Jeng, S. J.; Johnson, J.; Kannan, B.; Ke, Y.; Khan, B.; Kim, B.; Koswatta, S.; Kumar, A.; Kwon, T.; Kwon, U.; Lanzerotti, L.; Lee, H. K.; Lee, W. H.; Levesque, A.; Li,

DOI: 10.1021/acsami.6b13852
ACS Appl. Mater. Interfaces 2017, 9, 4948−4955

W.; Li, Z.; Liu, W.; Mahajan, S.; McStay, K.; Nayfeh, H.; Nicoll, W.; Northrop, G.; Ogino, A.; Pei, C.; Polvino, S.; Ramachandran, R.; Ren, Z.; Robison, R.; Saraf, I.; Sardesai, V.; Saudari, S.; Schepis, D.; Sheraw, C.; Siddiqui, S.; Song, L.; Stein, K.; Tran, C.; Utomo, H.; Vega, R.; Wang, G.; Wang, H.; Wang, W.; Wang, X.; Wehelle-Gamage, D.; Woodard, E.; Xu, Y.; Yang, Y.; Zhan, N.; Zhao, K.; Zhu, C.; Boyd, K.; Engbrecht, E.; Henson, K.; Kaste, E.; Krishnan, S.; Maciejewski, E.; Shang, H.; Zamdmer, N.; Divakaruni, R.; Rice, J.; Stiffler, S.; Agnello, P. High Performance 14 nm SOI FinFET CMOS Technology with 0.0174 um^2 Embedded DRAM and 15 Levels of Cu Metallization. In *IEEE International Electron Devices Meeting*; IEEE: Piscataway, NJ, 2014; pp 3.8.1−3.8.3.

(7) Natarajan, S.; Agostinelli, M.; Akbar, S.; Bost, M.; Bowonder, A.; Chikarmane, V.; Chouksey, S.; Dasgupta, A.; Fischer, K.; Fu, Q.; Ghani, T.; Giles, M.; Govindaraju, S.; Grover, R.; Han, W.; Hanken, D.; Haralson, E.; Haran, M.; Heckscher, M.; Heussner, R.; Jain, P.; James, R.; Jhaveri, R.; Jin, I.; Kam, H.; Karl, E.; Kenyon, C.; Liu, M.; Luo, Y.; Mehandru, R.; Morarka, S.; Neiberg, L.; Packan, P.; Paliwal, A.; Parker, C.; Patel, P.; Patel, R.; Pelto, C.; Pipes, L.; Plekhanov, P.; Prince, M.; Rajamani, S.; Sandford, J.; Sell, B.; Sivakumar, S.; Smith, P.; Song, B.; Tone, K.; Troeger, T.; Wiedemer, J.; Yang, M.; Zhang, K. In A 14 nm Logic Technology Featuring 2nd-Generation FinFET, Air-Gapped Interconnects, Self-Aligned Double Patterning and a 0.0588 um^2 SRAM Cell Size. In *IEEE International Electron Devices Meeting*; IEEE: Piscataway, NJ, 2014; pp 3.7.1−3.7.3.

(8) Wu, S. Y.; Lin, C. Y.; Chiang, M. C.; Liaw, J. J.; Cheng, J. Y.; Yang, S. H.; Chang, S. Z.; Liang, M.; Miyashita, T.; Tsai, C. H.; Chang, C. H.; Chang, V. S.; Wu, Y. K.; Chen, J. H.; Chen, H. F.; Chang, S. Y.; Pan, K. H.; Tsui, R. F.; Yao, C. H.; Ting, K. C.; Yamamoto, T.; Huang, H. T.; Lee, T. L.; Lee, C. H.; Chang, W.; Lee, H. M.; Chen, C. C.; Chang, T.; Chen, R.; Chiu, Y. H.; Tsai, M. H.; Jang, S. M.; Chen, K. S.; Ku, Y. In An Enhanced 16nm CMOS Technology Featuring 2nd Generation FinFET Transistors and Advanced Cu/Low-k Interconnect for Low Power and High Performance Applications. In *IEEE International Electron Devices Meeting*; IEEE: Piscataway, NJ, 2014; pp 3.1.1−3.1.4.

(9) Moore, G. E. Cramming More Components Onto Integrated Circuits. *Proc. IEEE* **1998**, *86* (1), 82−85.

(10) Zhang, H.; Duchaine, J.; Torregrosa, F.; Liu, L.; Holländer, B.; Breuer, U.; Mantl, S.; Zhao, Q. T. Improved NiSi Contacts on Si by CF_4 Plasma Immersion Ion Implantation for 14 nm Node MOSFETs. *2015 IEEE International Interconnect Technology Conference and 2015 IEEE Materials for Advanced Metallization Conference (IITC/MAM)*; IEEE: Piscataway, NJ, 2015; pp 187−190.

(11) Peter, A. P.; Meersschaut, J.; Richard, O.; Moussa, A.; Steenbergen, J.; Schaekers, M.; Tőkei, Z.; Van Elshocht, S.; Adelmann, C. Phase Formation and Morphology of Nickel Silicide Thin Films Synthesized by Catalyzed Chemical Vapor Reaction of Nickel with Silane. *Chem. Mater.* **2015**, *27* (1), 245−254.

(12) Kedzierski, J.; Ieong, M.; Kanarsky, T.; Zhang, Y.; Wong, H. S. P. Fabrication of Metal Gated FinFETs through Complete Gate Silicidation with Ni. *IEEE Trans. Electron Devices* **2004**, *51* (12), 2115−2120.

(13) Iwai, H.; Ohguro, T.; Ohmi, S.-i. NiSi Salicide Technology for Scaled CMOS. *Microelectron. Eng.* **2002**, *60* (1−2), 157−169.

(14) Lavoie, C.; d'Heurle, F. M.; Detavernier, C.; Cabral, C., Jr Towards Implementation of a Nickel Silicide Process for CMOS Technologies. *Microelectron. Eng.* **2003**, *70* (2−4), 144−157.

(15) Tang, W.; Picraux, S. T.; Huang, J. Y.; Gusak, A. M.; Tu, K.-N.; Dayeh, S. A. Nucleation and Atomic Layer Reaction in Nickel Silicide for Defect-Engineered Si Nanochannels. *Nano Lett.* **2013**, *13* (6), 2748−2753.

(16) Wang, H.; Zhang, Z.; Wong, L. M.; Wang, S.; Wei, Z.; Li, G. P.; Xing, G.; Guo, D.; Wang, D.; Wu, T. Shape-Controlled Fabrication of Micro/Nanoscale Triangle, Square, Wire-like, and Hexagon Pits on Silicon Substrates Induced by Anisotropic Diffusion and Silicide Sublimation. *ACS Nano* **2010**, *4* (5), 2901−2909.

(17) Li, Z.; Gordon, R. G.; Li, H.; Shenai, D. V.; Lavoie, C. Formation of Nickel Silicide from Direct-Liquid-Injection Chemical-Vapor-Deposited Nickel Nitride Films. *J. Electrochem. Soc.* **2010**, *157* (6), H679−H683.

(18) Kang, H.-S.; Ha, J.-B.; Lee, J.-H.; Choi, C. K.; Lee, J. Y.; Lee, K.-M. Effect of Catalyst for Nickel Films for NiSi Formation with Improved Interface Roughness. *Thin Solid Films* **2011**, *519* (20), 6658−6661.

(19) Dupre, C.; Hubert, A.; Becu, S.; Jublot, M.; Maffini-Alvaro, V.; Vizioz, C.; Aussenac, F.; Arvet, C.; Barnola, S.; Hartmann, J. M.; Garnier, G.; Allain, F.; Colonna, J. P.; Rivoire, M.; Baud, L.; Pauliac, S.; Loup, V.; Chevolleau, T.; Rivallin, P.; Guillaumot, B.; Ghibaudo, G.; Faynot, O.; Ernst, T.; Deleonibus, S. 15 nm-Diameter 3D Stacked Nanowires with Independent Gates Operation: ϕFET. In *2008 IEEE International Electron Devices Meeting*; IEEE: Piscataway, NJ, 2008; pp 1−4.

(20) Lee, K.-M.; Kim, C. Y.; Choi, C. K.; Yun, S.-W.; Ha, J.-B.; Lee, J.-H.; Lee, J. Y. Interface Properties of Nickel-Silicide Films Deposited by Using Plasma-Assisted Atomic Layer Deposition. *J. Korean Phys. Soc.* **2009**, *55* (31), 1153−1157.

(21) Ashcroft, A. T.; Cheetham, A. K.; Green, M. L. H.; Vernon, P. D. F. Partial Oxidation of Methane to Synthesis Gas Using Carbon Dioxide. *Nature* **1991**, *352* (6332), 225−226.

(22) Huber, G. W.; Shabaker, J. W.; Dumesic, J. A. Raney Ni-Sn Catalyst for H_2 Production from Biomass-Derived Hydrocarbons. *Science* **2003**, *300* (5628), 2075−2077.

(23) Besenbacher, F.; Chorkendorff, I.; Clausen, B. S.; Hammer, B.; Molenbroek, A. M.; Nørskov, J. K.; Stensgaard, I. Design of a Surface Alloy Catalyst for Steam Reforming. *Science* **1998**, *279* (5358), 1913−1915.

(24) Baudouin, D.; Szeto, K. C.; Laurent, P.; De Mallmann, A.; Fenet, B.; Veyre, L.; Rodemerck, U.; Copéret, C.; Thieuleux, C. Nickel−Silicide Colloid Prepared under Mild Conditions as a Versatile Ni Precursor for More Efficient CO_2 Reforming of CH_4 Catalysts. *J. Am. Chem. Soc.* **2012**, *134* (51), 20624−20627.

(25) Marciniec, B. *Hydrosilylation of Alkenes and Their Derivatives*; Springer: Dordrecht, The Netherlands, 2009; pp 3−51.

(26) Alphazan, T.; Mathey, L.; Schwarzwälder, M.; Lin, T.-H.; Rossini, A. J.; Wischert, R.; Enyedi, V.; Fontaine, H.; Veillerot, M.; Lesage, A.; Emsley, L.; Veyre, L.; Martin, F.; Thieuleux, C.; Copéret, C. Monolayer Doping of Silicon through Grafting a Tailored Molecular Phosphorus Precursor onto Oxide-Passivated Silicon Surfaces. *Chem. Mater.* **2016**, *28* (11), 3634−3640.

(27) Naftel, S. J.; Coulthard, I.; Sham, T. K.; Das, S. R.; Xu, D. X. Structural and Electronic Property Evolution of Nickel and Nickel Silicide Thin Films on Si(100) from Multicore X-ray-Absorption Fine-Structure Studies. *Phys. Rev. B: Condens. Matter Mater. Phys.* **1998**, *57* (15), 9179−9185.

(28) Park, J. Y.; Lee, H.; Renzas, J. R.; Zhang, Y.; Somorjai, G. A. Probing Hot Electron Flow Generated on Pt Nanoparticles with Au/TiO_2 Schottky Diodes during Catalytic CO Oxidation. *Nano Lett.* **2008**, *8* (8), 2388−2392.

(29) Lee, H.; Keun Lee, Y.; Nghia Van, T.; Young Park, J. Nanoscale Schottky Behavior of Au Islands on TiO_2 Probed with Conductive Atomic Force Microscopy. *Appl. Phys. Lett.* **2013**, *103* (17), 173103.

(30) Rose, A. Space-Charge-Limited Currents in Solids. *Phys. Rev.* **1955**, *97* (6), 1538−1544.

(31) Ravel, B.; Newville, M. ATHENA, ARTEMIS, HEPHAESTUS: Data Analysis for X-ray Absorption Spectroscopy Using IFEFFIT. *J. Synchrotron Radiat.* **2005**, *12* (4), 537−541.

DOI: 10.1021/acsami.6b13852
ACS Appl. Mater. Interfaces 2017, 9, 4948−4955